Tailoring the Structure of Two-Dimensional Self-Assembled Nanoarchitectures Based on Ni^{II}–Salen Building Blocks**

Marta Viciano-Chumillas, Dongzhe Li, Alexander Smogunov, Sylvain Latil, Yannick J. Dappe, Cyrille Barreteau, Talal Mallah, Fabien Silly

▶ **To cite this version:**

Marta Viciano-Chumillas, Dongzhe Li, Alexander Smogunov, Sylvain Latil, Yannick J. Dappe, et al.. Tailoring the Structure of Two-Dimensional Self-Assembled Nanoarchitectures Based on Ni^{II}–Salen Building Blocks**. Chemistry - A European Journal, 2014, 20 (42), pp.13566 - 13575. 10.1002/chem.201403169 . cea-01376984

HAL Id: cea-01376984
https://cea.hal.science/cea-01376984

Submitted on 3 Oct 2017

HAL is a multi-disciplinary open access archive for the deposit and dissemination of scientific research documents, whether they are published or not. The documents may come from teaching and research institutions in France or abroad, or from public or private research centers.

L'archive ouverte pluridisciplinaire **HAL**, est destinée au dépôt et à la diffusion de documents scientifiques de niveau recherche, publiés ou non, émanant des établissements d'enseignement et de recherche français ou étrangers, des laboratoires publics ou privés.

ChemPubSoc Europe

DOI: 10.1002/chem.201403169

CHEMISTRY
A European Journal
Full Paper

Self-Assembly

Tailoring the Structure of Two-Dimensional Self-Assembled Nanoarchitectures Based on Ni^{II}–Salen Building Blocks**

Marta Viciano-Chumillas,[a] Dongzhe Li,[b, c] Alexander Smogunov,[c] Sylvain Latil,[c] Yannick J. Dappe,[c] Cyrille Barreteau,[c, d] Talal Mallah,*[a] and Fabien Silly*[b]

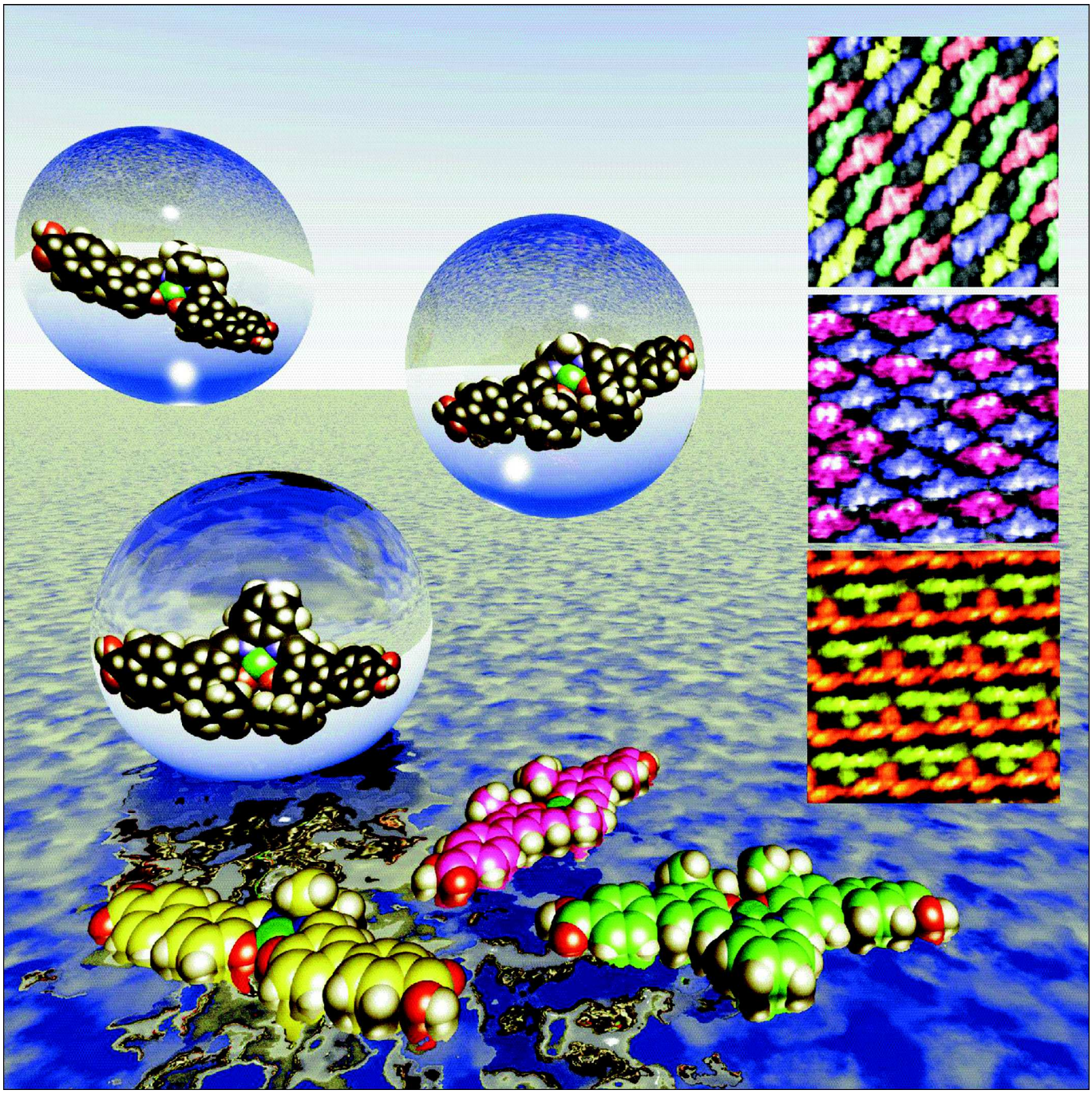

© 2014 Wiley-VCH Verlag GmbH & Co. KGaA, Weinheim

Abstract: The synthesis of a series of Ni^{II}–salen-based complexes with the general formula of $[Ni(H_2L)]$ ($H_4L = R^2$-*N*,*N*′-bis[R^1-5-(4′-benzoic acid)salicylidene]; H_4L1: $R^2 = 2,3$-diamino-2,3-dimethylbutane and $R^1 = H$; H_4L2: $R^2 = 1,2$-diaminoethane and $R^1 =$ *tert*-butyl and H_4L3: $R^2 = 1,2$-diaminobenzene and $R^1 =$ *tert*-butyl) is presented. Their electronic structure and self-assembly was studied. The organic ligands of the salen complexes are functionalized with peripheral carboxylic groups for driving molecular self-assembly through hydrogen bonding. In addition, other substituents, that is, *tert*-butyl and diamine bridges (2,3-diamino-2,3-dimethylbutane, 1,2-diaminobenzene or 1,2-diaminoethane), were used to tune the two-dimensional (2D) packing of these building blocks. Density functional theory (DFT) calculations reveal that the spatial distribution of the LUMOs is affected by these substituents, in contrast with the HOMOs, which remain unchanged. Scanning tunneling microscopy (STM) shows that the three complexes self-assemble into three different 2D nanoarchitectures at the solid–liquid interface on graphite. Two structures are porous and one is close-packed. These structures are stabilized by hydrogen bonds in one dimension, while the 2D interaction is governed by van der Waals forces and is tuned by the nature of the substituents, as confirmed by theoretical calculations. As expected, the total dipolar moment is minimized

Introduction

Engineering sophisticated metallo–organic nanoarchitectures on surfaces[1,2] is the focus of recent research interest for developing new catalysts[3] and new nanoarchitectures for spintronics.[4–10] Controlling molecular self-assembly offers unique directions for the fabrication of two-dimensional (2D) supramolecular nanoarchitectures[11,12] with specific electronic properties.[3,13] Self-assembled structures can be tailored at the nanometer scale by exploiting intermolecular interactions.[14–23] The molecular shape, size, structure, the nature and position of the substituent groups are key parameters governing the self-assembly of nanoarchitectures.[24–28] Researchers have therefore focused on synthesizing novel metallo–organic compounds (or coordination complexes) and developing innovative concepts for engineering new molecular nanoarchitectures that have tunable electronic properties and specific structures. Porphyrin and phtalocyanine complexes are archetypal systems that have been exhaustively investigated in the past.[29] Sedona et al., for example, engineered different nanoarchitectures based on iron–phthalocyanine to tune the catalytic activity of Ag(110).[3] Franke et al. showed that manganese–phthalocyanines adsorbed on Pb(111) form a spin −1 system that can lie in two different magnetic ground states.[7] Recently salen-based complexes (salen = *N*,*N*′-ethylenebis(salicylimine)) have been identified as a promising alternative to these cross-shaped iron–phthalocyanine and –porphyrin molecules to engineer 2D self-assembled metallo–organic nanoarchitectures.[30–34] The main advantages of metal–salen-based complexes (see Figure 1 a), apart from their quasi 2D molecular structure that is reminis-

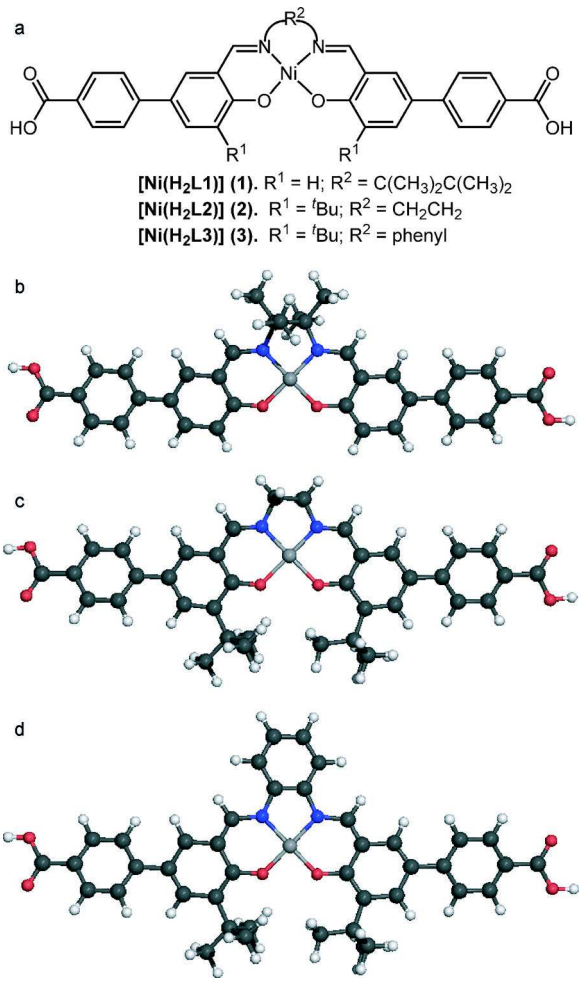

Figure 1. a) Nickel(II) complexes, $[Ni(H_2L)]$ (**1**–**3**). Crystal structure of complexes b) **1**, c) **2**, and d) **3**. Color code: Blue, nitrogen; red, oxygen; dark gray, carbon; light gray, nickel.

[a] *Dr. M. Viciano-Chumillas, Prof. T. Mallah*
Institute of Chemistry and Molecular Materials of Orsay
University of Paris Sud 11, 91405 Orsay (France)
E-mail: talal.mallah@u-psud.fr

[b] *D. Li, Dr. F. Silly*
IRAMIS, SPEC, TITANS, CNRS 2464
CEA, 91191 Gif-sur-Yvette (France)
E-mail: fabien.silly@cea.fr

[c] *D. Li, Dr. A. Smogunov, Dr. S. Latil, Dr. Y. J. Dappe, Dr. C. Barreteau*
IRAMIS, SPEC, MSIN, CNRS 2464
CEA, 91191 Gif-sur-Yvette (France)

[d] *Dr. C. Barreteau*
DTU NANOTECH, Technical University of Denmark
Ørsteds Plads 344, 2800 Kgs. Lyngby (Denmark)

[**] *Salen* = N,N′-*Ethylenebis(salicylimine)*

© 2014 Wiley-VCH Verlag GmbH & Co. KGaA, Weinheim

cent of porphyrins and phtalocyanines, are their chemical versatility and flexibility.[35–37] A broad variety of metal ions (dia- and paramagnetic) can be introduced in the coordination pocket without altering the molecular skeleton. Numerous substituents can in addition be placed around the phenol rings and on the diamine bridge. The *para*-position of the salen phenol ring can be used to introduce suitable substituents to drive molecular self-assembly into one-dimensional (1D) salen chains. In comparison the *ortho*-position of the salen phenol ring and the diamine bridge can be used to attach substituents not only for driving molecular self-assembly, but also for tuning salen/central-metal-ion surface separation and therefore metal-ion surface electronic coupling. The benefit of such functionalization is that substituents are usually located close to the central metal ion. One therefore expects to be able to tune molecular electronic properties by replacing the substituents. These substituents may not only influence molecular self-assembly, but may also modify the electronic properties of the complexes. Recent research effort has been focused on metal–salen complexes syntheses for developing efficient catalysts for the separation of acetylene and ethylene[38] or the selective oxygenation of organic sulfides,[39–43] sulfoxides,[43,44] and heteroatom-containing organic compounds.[45] It has been shown that modifying the structure of these complexes drastically affects the chemical reaction. Catalytic selectivity and activity can be improved by changing the central metal ion or the ligands, that is, catalytic activity can be tuned by introducing substituents in the 3- and 5-positions of the salen ligand.[45] Salen derivatives can also play an important role in spintronics and nanotechnology, because magnetic metal ions can be implanted inside the molecular skeleton. For example, Dilullo et al. observed the appearance of an antiferromagnetic exchange coupling between the spin centers in a covalent salen chain.[46] Future technological developments based on salen molecules require a precise control of their molecular electronic properties as well as their molecular assembly to optimize and tailor the properties of the 2D nanoarchitectures.

Herein we report the preparation of three nickel(II) complexes with the general formula [Ni(H_2L)] (H_4L = R^2-*N*,*N*′-bis(R^1-5-(4′-benzoic acid)salicylidene); H_4L1: R^2 = 2,3-diamino-2,3-dimethylbutane and R^1 = H; H_4L2: R^2 = 1,2-diaminoethane and R^1 = *tert*-butyl and H_4L3: R^2 = 1,2-diaminobenzene and R^1 = *tert*-butyl), as shown in Figure 1. Different substituents have been placed on the diamine bridge and at the 3-position of the phenol ring. We have used DFT calculations to elucidate how the presence of these substituents affects the electronic properties of these building blocks. We then used scanning tunneling microscopy to investigate the influence of the substituents on the self-assembly. We observed that the three molecular building blocks self-organize into three different organic nanoarchitectures. The difference in the 2D molecular arrangements was rationalized with the help of theoretical calculations.

Results and Discussion

Synthesis

The salen scaffold was functionalized with benzoic acid and *tert*-butyl groups placed at the *para*- and *ortho*-positions of the phenol rings, respectively, and as well as different diamine bridges. The reaction between Ni($OAc)_2$·4H_2O and the corresponding carboxylic salen derivative H_4L (Figure 1) in a mixture of methanol and dimethylformamide under reflux affords the complexes **1**–**3** with the general formula [Ni(H_2L)]. The complexes were characterized by IR and NMR spectroscopy and mass spectrometry. In addition, single crystals of compound **1** suitable for X-ray diffraction analysis were also obtained, showing the presence of chains due to the hydrogen bonding. The IR spectrum of compounds **1**–**3** exhibit a strong band at around 1680 cm^{-1}, indicating the presence of the acid carboxylic groups of the salen ligand.

Modeling electronic properties

We used DFT calculations (see Experimental Section) to assess the electronic properties of complexes **1**–**3**. The total density of states (DOS), $\rho(\varepsilon) = \sum_i \delta(\varepsilon - \varepsilon_i)$, and the projected DOS (PDOS), $\rho_\alpha(\varepsilon) = \sum_i |\langle \phi_\alpha \mid \phi_i \rangle|^2 \delta(\varepsilon - \varepsilon_i)$, onto different 3d Ni orbitals, ϕ_α, are presented for each complex in Figure 2. For better visualization, all δ-like peaks are broadened with a small parameter. Calculations show that the HOMO–LUMO energy gaps Δ are affected by the nature of the substituents and ranges from $\Delta \approx 1.3$ eV (complex **2**) to $\Delta \approx 1.5$ eV (complex **1**). One should take with care these absolute values, since it is

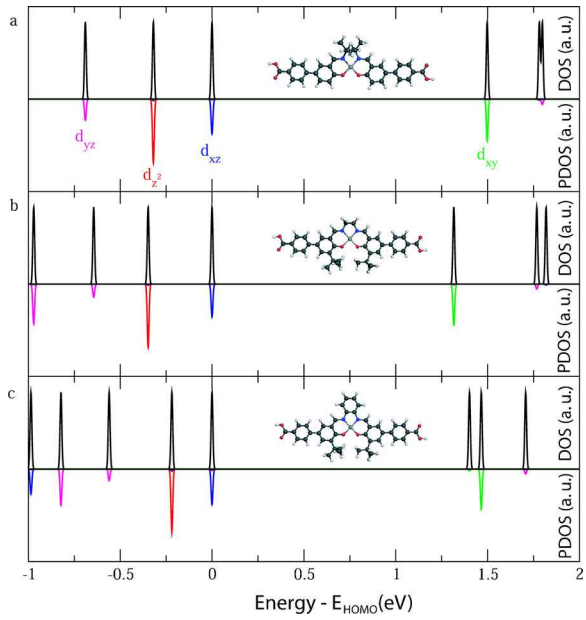

Figure 2. Calculated density of states of complexes a) **1**, b) **2**, and c) **3**. For each molecule we present the total DOS (set to positive values) as well as the DOS projected on different atomic orbitals of Ni^{II} ion, the PDOS (set to negative values). The energy onset is set to the position of the HOMO orbital.

© 2014 Wiley-VCH Verlag GmbH & Co. KGaA, Weinheim

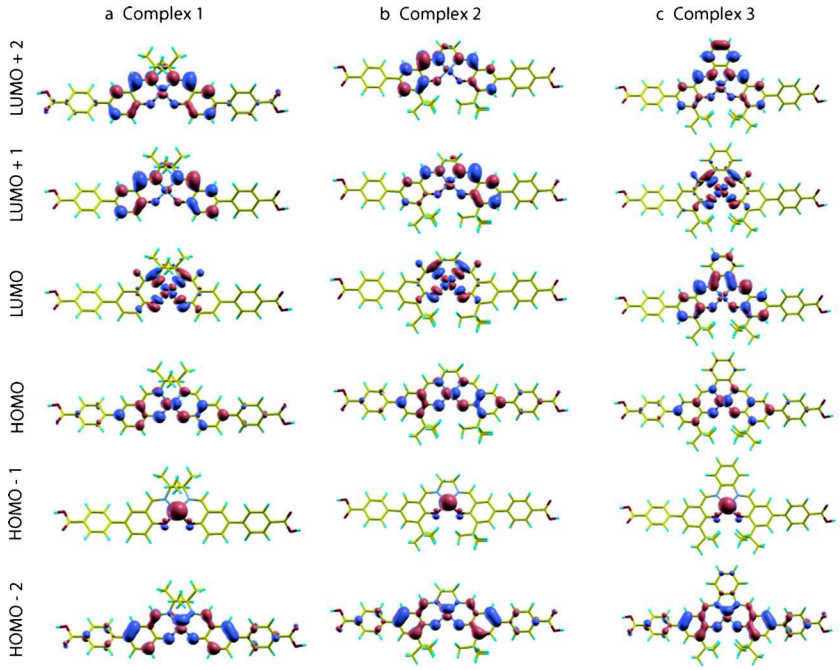

Figure 3. Calculated spatial distributions of different molecular orbitals for the complexes a) **1**, b) **2**, and c) **3**. Isosurfaces of positive (0.001) and negative (−0.001) isovalues are shown in red and blue, respectively.

known that the mean-field DFT calculations tend generally to underestimate the energy gaps, while the relative trend (complex **2** has the smallest band gap and complex **1** has the largest one) is expected to be correct.

The spatial distributions of different molecular orbitals are shown in Figure 3. The calculated molecular orbital maps of the HOMO, HOMO−1, and HOMO−2 states are rather similar for the three molecular complexes so that molecular substituents do not have a noticeable influence. For each complex, the HOMO−1 is heavily localized on the Ni d_{z^2} orbital pointing out of the molecular plane, while the HOMO orbital is associated with another out of plane Ni orbital, d_{xz}. These observations agree of course with the PDOS spectra shown in Figure 2. In contrast with the HOMO orbitals, calculations reveal that the unoccupied orbitals (LUMO, LUMO+1) are affected by the molecular substituents. The LUMO orbitals of complexes **1** and **2** are very similar and are mainly localized on the Ni d_{xy} orbital (see also Figure 2a,b). In contrast, the LUMO orbital of complex **3** has a very small weight on the Ni atom. A careful comparison of molecular orbital spatial distributions shows that the LUMO orbital of complexes **1** and **2** is instead similar to the LUMO+1 orbital of complex **3** (Figure 2c). This difference in unoccupied molecular orbitals is mainly caused by the central substituent R^2, for which these orbitals have significant weight. Moreover, the substituent R^2 for complexes **1** and **2** is asymmetric with respect to the *xz* plane passing through the center of the molecule and perpendicular to its plane. Therefore, the states will not in general be purely even or odd with respect to the *xz* plane, which is clearly seen for LUMO+1 and LUMO+2 orbitals of complex **2**. This mixing of even/odd symmetries seems, however, to be much weaker for the complex **1**, which is also reflected in the smaller LUMO+2–LUMO+1 splitting compared to that in complex **2**. It should be possible to experimentally image molecular HOMOs and LUMOs using mode-lock-in scanning tunneling spectroscopy at very low temperature.

The difference between the unoccupied molecular orbitals of the different complexes can be explained using a simple Hückel analysis of the sp^2-carbon molecular skeleton. Complex **3** contains a fully aromatic diamine bridge (1,2-diaminobenzene), whereas complexes **1** and **2** are constructed with sp^3-carbon-atom-based bridges, acting as barriers breaking the overall sp^2 character that can no longer spread over the entire molecule. The eigenstates resulting from the coupling between the metal ion and the *p*-delocalized networks of the surrounding ligands will therefore be similar for these two complexes. The carbon sp^2 skeleton of complex **3** is in comparison fully connected and contains six supplementary carbon atoms, resulting in six extra p orbitals that interact with the 3d shell of the metal ion. This complex is fully sp^2. The corresponding schemes are illustrated in Figure 4.

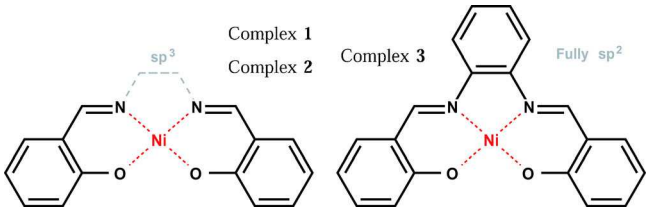

Figure 4. Hückel sp^2 schemes of complexes **1** and **2**. Right: carbon sp^2 skeleton of the complex **3**.

Salen Two-Dimensional Nanoarchitectures

Complex 1 self-assembly

The STM images were performed at the solid–liquid interface using freshly cleaved HOPG (highly oriented pyrolytic graphite) substrates (see Experimental Section). STM images (Figure 5a,b) show that complex **1** self-assembles into large domains at the liquid–graphite interface. Molecules are colored in green, red, blue, and yellow in the high-resolution STM image (Figure 5b) to highlight the four distinctive orientations adopted by the molecules. The images reveal a porous 2D organization as modeled in Figure 5c. The organic network has an oblique unit cell with (5.1±0.4) and (1.9±0.2) nm unit cell parameters and an angle of (87±5)° between the two directions

© 2014 Wiley-VCH Verlag GmbH & Co. KGaA, Weinheim

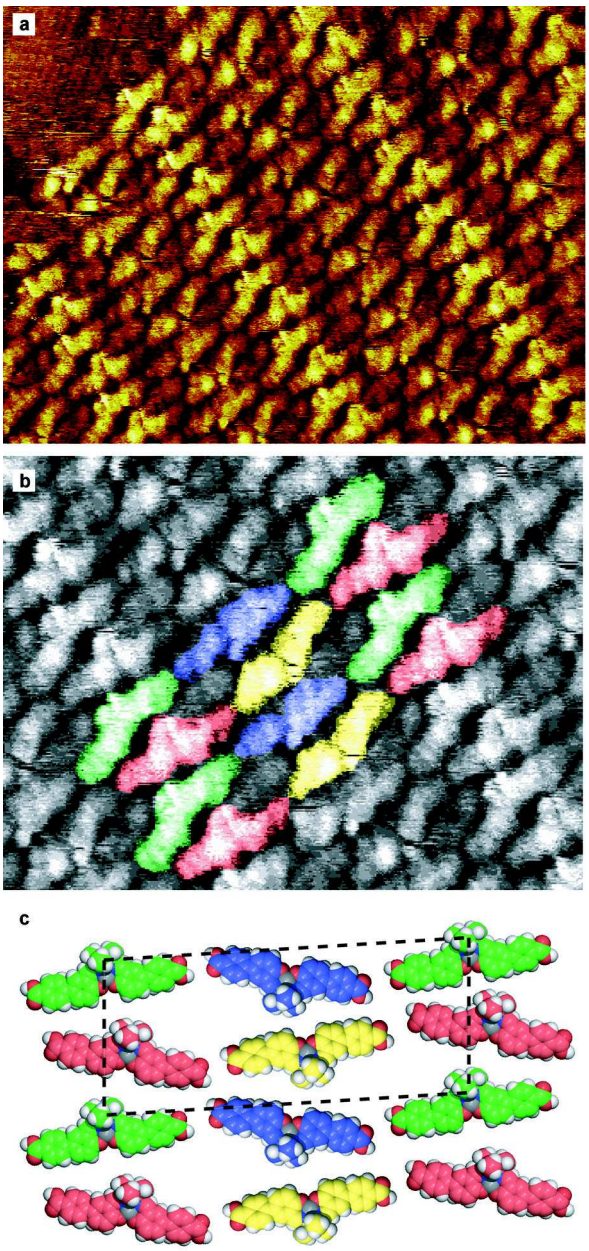

Figure 5. STM images of complex **1** domain on graphite: a) 15×11 nm^2, V_s=0.75 V; b) 10×7 nm^2, V_s=0.75 V, I_t=53 pA. In b) blue, green, red, yellow colored molecules show their four orientations in the organic layer. c) Complex **1** network model. Color code: Blue, nitrogen; red, oxygen; white, hydrogen; light gray, nickel. Carbon atoms are blue, green, red or yellow depending of the molecule orientation.

(Figure 5c). This structure is composed of parallel chains stabilized by hydrogen bonds between carboxylic groups. Molecules are rotated by an angle of 160° along the chains. This leads to the formation of a zigzag 1D arrangement. The molecules of neighboring chains are rotated by an angle of 180° (blue and yellow molecules are rotated by 180° with respect to green and red molecules). The 2,3-diamino-2,3-dimethyl butane bridge (position R^2 in Figure 1) of each molecule is alternatively facing one of the hydrogen atoms located at the position of R^1 in a molecule of the neighboring chain. Cavities are thus formed between green–blue and red–yellow paired molecules.

Complex 2 self-assembly

The large-scale STM image (Figure 6a) shows that complex **2** (Figure 1b) self-assembles at the liquid/graphite interface into a compact 2D network. In comparison with **1**, the assembly of **2** results from the close-packing of straight molecular chains,

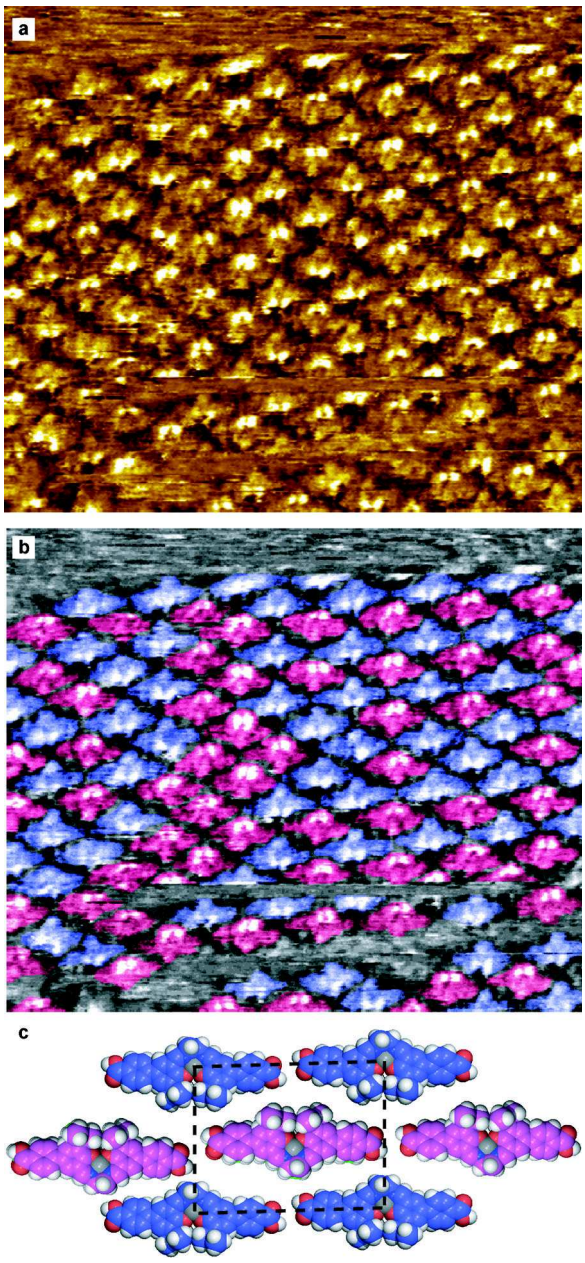

Figure 6. a) STM image of complex **2** self-assembled domain on graphite, 20×14 nm^2, V_s=0.8 V, I_t=35 pA. b) Molecules are colored in blue or purple false color according to their orientation. c) Model of the complex **2** network. Color code: blue, nitrogen; red, oxygen; white, hydrogen; light gray, nickel. Carbon atoms are purple or blue depending of the molecule orientation.

© 2014 Wiley-VCH Verlag GmbH & Co. KGaA, Weinheim

as previously observed.[47] These chains are also stabilized by hydrogen bonds between the carboxylic groups.

Neighboring chains are shifted along their axis by a distance equal to the half-molecule length. Two molecular orientations are observed in the network. They are related by an angle of 180° along the chain axis. In Figure 6a, molecules are colored in purple and blue according to their orientation. It appears that molecules preferentially adopt the same orientation along the organic chain and that molecules of neighboring chains have the opposite orientation (corresponding to a rotation of 180°). A model of the nanoarchitecture derived from complex **2** is presented in Figure 6b. The network unit cell is a parallelogram with (2.6±0.3) and (1.6±0.2) nm unit cell edges forming an angle of (83±5)° between them. Defects are, however, visible in the structure in Figure 6a, that is, about 30% of the molecules are rotated by an angle of 180° in comparison with the main orientation of the molecule along the chain. However, this does not lead to the appearance of cavities in the structure, that is, the close-packing is preserved. Overall Figure 6a shows that 64 molecules are oriented "up" (blue) and 64 molecules are oriented in the opposite direction (purple). Molecules can easily be separated from the domain edge by the STM tip during scanning. This is why they are sometimes partially resolved in STM images (bottom of the Figure 6a).

Complex 3 self-assembly

The large-scale STM image (Figure 7a) shows that molecules of **3** self-assemble into an open 2D network at the liquid–graphite interface. Figure 7b shows a high-resolution STM image of the edge of complex **3** network. As it was observed for **2**, complex **3** adopts two orientations. These orientations are related by a 180° rotation angle along the molecular chain axis. Molecules have been colored in green and in red according to their orientation in Figure 7b. The nanoarchitecture of complex **3** consists thus of the packing of straight molecular chains. These chains are again stabilized by the hydrogen bonds formed between the carboxylic groups of neighboring molecules as for the other cases. In contrast with complex **2**, neighboring molecules strictly adopt the same orientation along the chain. The molecules of the neighboring chains are oriented in the opposite direction (rotation of 180°). Neighboring chains are in addition shifted along their axis by a distance nearly equivalent to half-molecule length. The 1,2-diaminobenzene is thus pointing to the carboxylic groups of the molecules of the neighboring chain. This leads to the appearance of square cavities between the benzene groups of molecules of neighboring chains. The *tert*-butyl groups of molecules of neighboring chains are next to each other. The model of this structure is presented in Figure 7c. The network unit cell is highlighted by dashed lines. It is a parallelogram with (2.6±0.3) and (1.8±0.2) nm unit cell edges forming an angle of (85±5)° between them. Square cavities between the benzene groups of molecules of neighboring chains are formed.

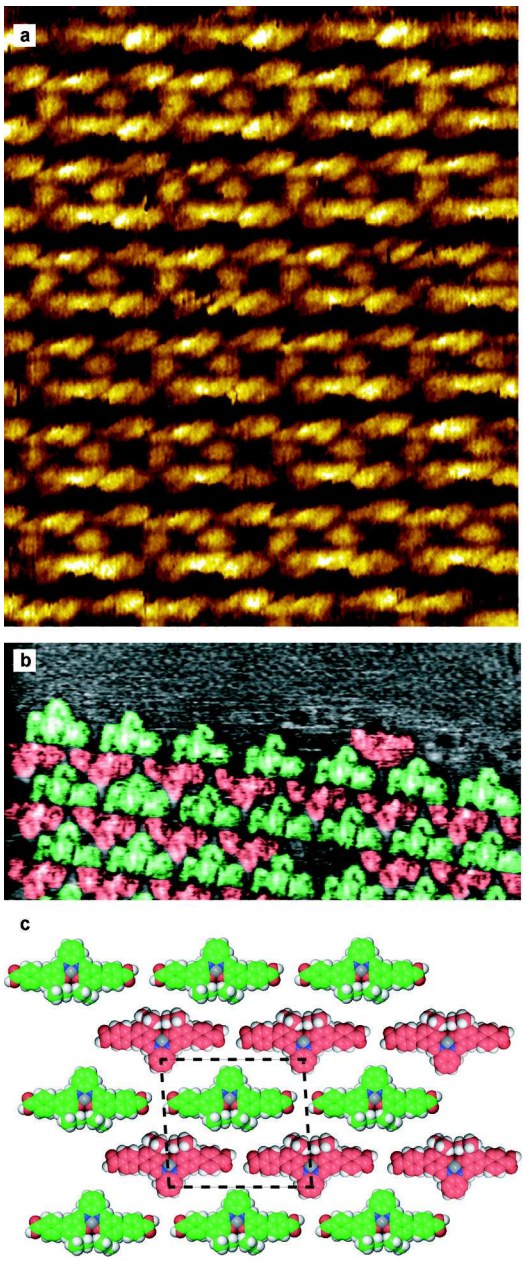

Figure 7. High resolution STM image of complex **3** domain on graphite: a) 14×12 nm², V_s=0.70 V, I_t=8 pA; b) 18×9 nm², V_s=0.70 V, I_t=8 pA. Red and green colored molecules show their two orientations in the organic layer. c) Model of nanoarchitecture of complex **3**. Color code: blue, nitrogen; red, oxygen; white, hydrogen.

Intermolecular features

High-resolution STM images of individual complexes **1**–**3** (Figure 8) reveal some intramolecular features. The 2,3-diamino-2,3-dimethylbutane bridge in complex **1** and the *tert*-butyl groups in complexes **2** and **3** appear as bright spots in the STM images as shown in Figure 8a–c, respectively. These substituents are thus not lying flat on the surface. In contrast with complex **1**, the diamine bridges of complexes **2** and **3** are nearly flat. Therefore, they have the same contrast as the skeleton in the STM images.

© 2014 Wiley-VCH Verlag GmbH & Co. KGaA, Weinheim

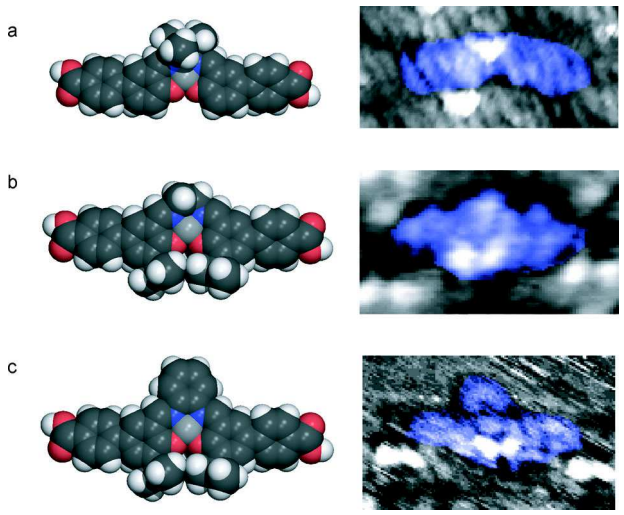

Figure 8. Left column: model of complexes a) **1**, b) **2**, and c) **3**. Right column: high-resolution STM images of a) complex **1**, 4×1.8 nm^2; $V_s=0.82$ V, $I_t=35$ pA; b) complex **2**, 4×2.1 nm^2; $V_s=0.78$ V, $I_t=115$ pA; and c) complex **3**, 4×2.5 nm^2; $V_s=0.72$ V, $I_t=127$ pA.

Salen nanoarchitecture energy

The STM images show that complexes **1**–**3** form self-assembled nanoarchitectures composed of parallel chains on graphite. The chains are stabilized by the hydrogen bonds between the carboxylic groups of neighboring molecules. The chains in complexes **2** and **3** are straight, but surprisingly the chains in complex **1** adopt a zig-zag configuration. The LCAO-S^2+vdW formalism (see Experimental Section) has been used to determine the structural and energetic properties of the assemblies of **1**–**3**. The molecular structures and unit cells have been defined in agreement with the experimental observations presented in Figures 5 and 7. Calculations reveal that the binding energy of the complex **1** tilted network is −1.216 eV per molecule, while it is much lower for the assemblies derived from complexes **2** and **3** (−495 and −577 meV per molecule, respectively) for which straight structures were observed (Table 1). The three nanoarchitectures are therefore stable. The lowest energy structure was found for complex **1**, despite the 1D zigzag configuration that weakens the double hydrogen bonds between the carboxylic groups. However, this structure maximizes van der Waals interactions between molecules of neighboring chains, that is, molecular arms are placed side by side. In comparison the energy of an assembly of complexes **1** with a straight 1D chains structure was found to be equal to −688 meV per molecule. The straight arrangement of complex **1** is therefore less favorable than the zigzag configuration and the van der Waals forces between adjacent chains are the key-point for the stabilization of observed arrangement.

Nanoarchitecture dipolar moment

Intermolecular dipole interactions can influence molecular self-assembly.[48–51] Salen complexes are known to be polar molecules, since they possess a permanent dipole moment. It is displayed along the direction of the twofold symmetry axis bisecting the OMO and the NMN angles.[32] The nanoarchitectures of complexes **1**–**3** are all composed of parallel chains. In complex **1**, molecules are alternatively rotated by about 160° along chain axis, and molecules of neighboring chains are nearly aligned in the same direction. This leads to the appearance of dipolar rows, the axis of which is almost perpendicular to the chain axis. Neighboring dipolar rows have opposite orientation. This is represented in Figure 9a.

In comparison with complex **1**, complex **2** has the same orientation along the molecule chain axis, but molecules of neighboring chains are rotated by 180°. In addition neighboring chains are shifted along the axis. This also leads to the appearance of dipolar rows, the axis of which is perpendicular to the chain axis. Neighboring dipolar rows have opposite orientation. This is represented in Figure 9b. The separation of electric dipoles in complex **2** is twice as small as the dipole separation in complex **1**. Since the self-assembly of complexes **2** and **3** is similar, the resulting dipole distribution in the complex **3** structure is identical to the dipole distribution for the structure derived from **2**, see Figure 9c. Figure 9 shows that self-assembled complexes **1**–**3** lead to the formation of electric dipoles on the surface, but the overall dipole moment in the three salen nanoarchitectures is minimized. This is also the case in the complex **2** self-assembly. This structure is the only one that has defects, that is, a few molecules along molecular chains have opposite orientation. However, Figure 6 shows that 50% of the molecules adopt the "up" orientation and the rest adopt the "down" orientation. The total dipole moment is therefore also minimized despite defects induced by molecular incorrect

Table 1. Nanoarchitecture structure and energy.

	Complex **1**		Complex **2**	Complex **3**
cell	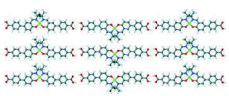	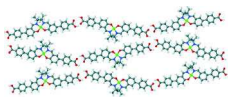	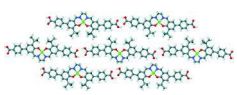	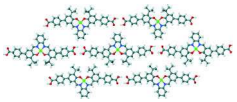
packing	porous	porous	close-packed	porous
orientation	straight	zigzag	straight	straight
energy per mol [meV mol^{-1}]	−688	−1216	−495	−577
energy per nm^2 [meV nm^{-2}]	−237.5	−491.8	−236.5	−174.3

© 2014 Wiley-VCH Verlag GmbH & Co. KGaA, Weinheim

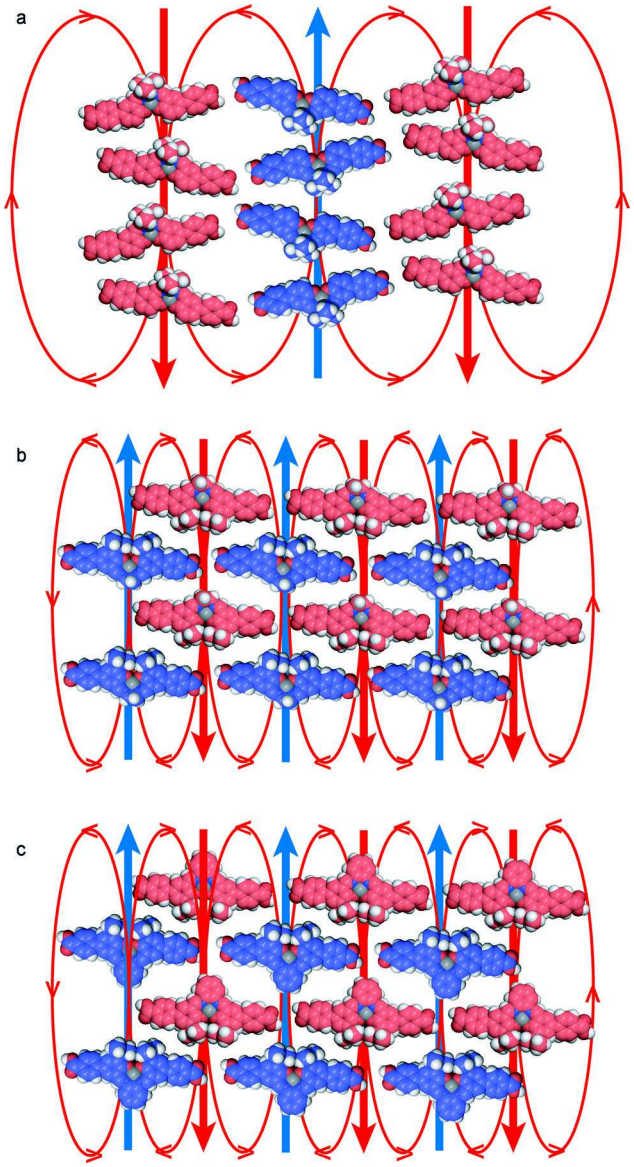

Figure 9. Nanoarchitectures of complexes a) **1**, b) **2**, and c) **3** showing the dipolar lines. Molecules are colored according to their "up" (blue) and "down" (red) structural orientation. The resulting electric dipoles are represented by blue (up orientation) and red (down) arrows.

orientation. In addition, this observation also suggest that intermolecular dipolar interactions govern the orientation of closest neighbors in complex **2** structure and stabilize the unit cell presented in Figure 6c, as mentioned previously.[47]

Conclusions

In summary we synthesized Ni^{II}–salen derivative complexes with several diamine bridges, that is, 2,3-diamino-2,3-dimethylbutane (**1**), 1,2-diaminoethane (**2**), and 1,2-diaminobenzene (**3**), with a hydrogen or *tert*-butyl group at the 6-position of the phenol ring. Additionally all ligands were functionalized with benzoic groups at the *para*-position of the phenol ring. DFT calculations reveal that substituents affect both the molecular band gap and the LUMO orbitals, but leaving the HOMO states almost unchanged. STM measurements shows that porous networks and close-packed nanoarchitectures can be engineered using these building blocks. These nanoarchitectures are stabilized by hydrogen bonds, van der Waals, and molecular dipolar interactions. The interplay between the different forces has an important impact on the overall nanoarchitecture structure. An exciting perspective of this work consists in exploring the catalytic[3] and magnetic[46] properties of these two-dimensional nanoarchitectures based on salen complexes.

Experimental Section

General

4-(3-Hydroformyl-4-hydroxy-phenyl)bezoic acid,[52] 4-(3-hydroformyl-4-hydroxy-5-*tert*-butyl-phenyl)bezoic acid,[52] and 2,3-diamino-2,3-dimethylbutane[34] were synthesized according to reported procedures. Complex **2** was prepared as reported previously.[47] Starting materials were purchased from Aldrich and all manipulations were performed using materials as received.

Physical measurements

^{1}H NMR spectra were recorded on a Bruker 300 MHz spectrometer. All chemical shifts are reported in ppm and are referenced to deuterated DMSO ($\delta = 2.50$ ppm). IR spectra (4000–300 cm^{-1}) were recorded as KBr pellets on a PerkinElmer FTID 1000 spectrometer. Mass analyses in tetrahydrofurane were recorded on a Perseptive Voyager DE STR MALDI TOF-MS spectrometer. Elemental analyses for C, H and N were determined by the Service de Microanalyses, ICSN-CNRS, Gif-sur-Yvette (France).

General synthetic procedures

General procedure for the synthesis of H_4L: The respective diamine (0.75 mmol) and few drops of ethylorthoformate were added to a solution of 4-(3-hydroformyl-4-hydroxy-phenyl)benzoic acid (1.50 mmol) or 4-(3-hydroformyl-4-hydroxy-5-*tert*-butyl-phenyl)benzoic acid (1.50 mmol) in ethanol (50 mL). The reaction mixture was stirred under reflux for 2 h. The solvent was removed under reduced pressure. The solid was sonicated with diethyl ether filtered, and dried under vacuum.

H_4L1: Yield: 78%; ^{1}H NMR (300 MHz, [D_6]DMSO): $\delta = 1.38$ (s, 6H; -C(CH_3)$_2$), 6.95 (d, $J = 8.4$ Hz, 1H; Ar-*H*), 7.73 (s, 1H; Ar-*H*), 7.77 (d, $J = 10.2$ Hz, 2H; Ar-*H*), 7.98 (s, 3H; Ar-*H*), 8.76 (s, 1H; -*CH*=N-), 12.35 (br s, 1H; -CO_2*H*), 14.35 ppm (s, 1H; -O*H*); IR: $\tilde{\nu} = 3437$ (br), 2985 (w), 1678 (s), 1628 (s), 1606 (s), 1521 (w), 1488 (m), 1423 (m), 1378 (m), 1298 (m), 1281 (m), 1244 (m), 1284 (m), 1122 (m), 1015 (w), 987 (w), 944 (w), 827 (m), 773 (m), 728 (w), 551 cm^{-1} (w); MS (MALDI-TOF): *m/z* calcd for $[M+H]^+$: 565.23; found: 565.24.

H_4L3: Yield: 41%; ^{1}H NMR (360 MHz, [D_6]DMSO): δ 1.45 (s, 9H; -C(CH_3)$_3$), 7.48 (m, 1H; Ar-*H*), 7.59 (m, 1H; Ar-*H*), 7.70 (s, 1H; Ar-*H*), 7.79 (d, $J = 8.28$ Hz, 2H; Ar-*H*), 7.95 (s, 1H; Ar-*H*), 8.02 (d, $J = 7.92$ Hz, 2H; Ar-*H*), 9.12 (s, 1H; -*CH*=N-), 12.92 (br s 1H; -CO_2*H*), 14.26 ppm (s, 1H; -O*H*); IR: $\tilde{\nu} = 3437$ (br), 2955 (w), 1686 (s), 1606 (s), 1571 (s), 1484 (m), 1468 (m), 1437 (m), 1423 (m), 1393 (m), 1363 (m), 1271 (m), 1250 (m), 1230 (m), 1168 (m), 1108 (m), 1072 (w), 1048 (w), 1015 (w), 975 (w), 931 (w), 879 (w), 849 (m), 773 (m), 750 (m), 550 (w), 494 cm^{-1} (w); MS (MALDI-TOF): *m/z* calcd for $[M+H]^+$: 669.30; found: 669.28.

General procedure for the synthesis of [Ni(H_2L)]: A solution of Ni(OAc)$_2$·4H_2O (0.15 mmol) in methanol (5 mL) was added to a solu-

© 2014 Wiley-VCH Verlag GmbH & Co. KGaA, Weinheim

tion of the ligand H_4L (0.15 mmol) in dimethylformamide/methanol (20 mL). The reaction mixture was stirred for 1 h at 80 °C. After slow evaporation of the solvent, a crystalline red precipate was formed. The precipitate was filtered and washed with methanol (5 mL), and dried in vacuo.

[Ni(H_2L1)] (1): Yield: 82%; ^{1}H NMR (300 MHz, [D_6]DMSO): $\delta = 1.44$ (s, 6H; -CH_3-), 6.83 (d, $J = 8.70$ Hz, 1H; Ar-*H*), 7.66 (dd, $J = 8.85$, 2.1 Hz, 1H; Ar-*H*), 7.73 (d, $J = 8.4$ Hz, 2H; Ar-H), 7.95 (s, 2H; Ar-*H*), 7.98 (s, 1H; -C*H*=N-), 8.00 (s, 1H; Ar-*H*), 12.85 ppm (s, 1H; -CO_2*H*); IR: $\tilde{\nu} = 3434$ (br), 2972 (w), 1685 (s), 1674 (s), 1617 (m), 1598 (s), 1533 (m), 1514 (w), 1473 (m), 1422 (m), 1388 (s), 1317 (m), 1287 (s), 1249 (s), 1187 (s), 1148 (s), 1129 (m), 1014 (w), 946 (w), 923 (w), 853 (w), 830 (m), 774 (m), 730 (m), 659 (w), 647 (w), 607 (w), 536 (m), 463 cm^{-1} (w); MS (MALDI-TOF): *m/z* calcd for $[M+H]^+$: 621.15; found: 621.13; elemental analysis calcd (%) for **1**·1.3 DMF ($C_{34}H_{30}N_2NiO_6$·1.3 DMF): C 63.55, H 5.5, N 6.45; found: C 62.68, H 5.30, N 6.09.

[Ni(H_2L3)] (3): Yield: 86%; ^{1}H NMR (250 MHz, [D_6]DMSO): $\delta = 1.47$ (s, 9H; -C(CH_3)$_3$), 7.37 (m, 1H; Ar-*H*), 7.63 (s, 1H; Ar-*H*), 7.75 (d, $J =$ 8.25 Hz, 2H; Ar-*H*), 7.99 (s, 2H; Ar-*H*), 8.03 (s, 1H; Ar-H), 8.18 (m, 1H; Ar-*H*), 9.01 (s, 1H; -C*H*=N-), 12.85 ppm (s, 1H; -CO_2*H*); IR: $\tilde{\nu} =$ 3436 (br), 2946 (w), 1682 (s), 1600 (s), 1579 (s), 1533 (s), 1492 (w), 1466 (w), 1419 (m), 1389 (s), 1293 (m), 1240 (m), 1179 (m), 1101 (w), 898 (w), 846 (m), 816 (w), 771 (m), 557 cm−1 (w); MS (MALDI-TOF): *m/z* calcd for $[M+H]^+$: 725.22; found: 725.26; elemental analysis calcd (%) for **3**·1 DMF ($C_{42}H_{38}N_2NiO_6$·1 DMF): C 67.68, H 5.68, N 5.26; found: C 67.79, H 5.33, N 4.36.

STM studies

Solutions of complexes **1** and **3** in 1-octanol (99%, Acros) were prepared. A droplet of these solutions was then deposited on a freshly cleaved highly ordered pyrolytic graphite (HOPG) substrate. STM imaging of the samples were performed at the liquid–solid interface using a Pico-STM scanning tunneling microscope (Molecular Imaging, Agilent Technology). Mechanically etched Pt/Ir wires were used to obtain constant current images at room temperature with a bias voltage applied to the sample. STM images were processed and analyzed using the application FabViewer.[53]

DFT calculations

The structural and the energetic properties of the complexes **1**–**3** were calculated with the LCAOS^2+vdW formalism. This approach is based on DFT in combination with an intermolecular perturbation theory to describe weak and van der Waals (vdW) interactions. The DFT computational scheme, as well as the theoretical foundations underlying our calculations—a very efficient DFT localized orbital molecular dynamics technique (FIREBALL)—have been described in full detail elsewhere.[54–57] Each individual molecule was analyzed by using a self-consistent version of the Harris–Foulkes LDA functional,[58,59] instead of the traditional Kohn–Sham (KS) functional based on the electronic density, whereby the KS potential is calculated by approximating the total charge by a superposition of spherical charges around each atom. The FIREBALL simulation package uses a localized optimized minimal basis set,[60] and the self-consistency is achieved over the occupation numbers through the Harris functional.[61] In addition, the LDA exchange-correlation energy was calculated by using the efficient multicenter-weighted exchange-correlation density approximation (McWEDA).[55,56] Two intermolecular "weak interactions" for each specific configuration, which can be seen as two opposite contributions, were added to these DFT calculations. The first one, named "weak chemical" interaction is due to the small overlaps between molecular electronic densities. Therefore, this energy can be determined as an expansion of the wave-functions and operators with respect to these overlaps. This expansion is based on a development in S^2 (since in the weak interacting case the overlaps are really small) of the $S^{1/2}$ term appearing in the Löwdin orthogonalization, which induces a shift of the occupied eigen energies of each independent molecule, and leads to a repulsive energy between them. The second contribution is the pure van der Waals interaction, which finds its origin in charge fluctuations, arising from oscillating dipoles, the interaction of which gives the attractive part of the cohesive energy. This interaction was treated in the dipolar approximation, and added in perturbation to the total energy of the molecular assemblies. The balance of the two contributions gave the equilibrium configuration of the system. This formalism[62,63] has already provided excellent results in the study of a wide range of graphitic and molecular materials.

DFT calculations were performed by using ab-initio plane-wave electronic structure package Quantum-ESPRESSO.[64] The generalized gradient approximation for exchange-correlation potential in the Perdew, Burke, and Ernzerhof parametrization[65] was employed and the interactions between valence electrons and atomic cores were described by ultrasoft pseudopotentials.[66] All atomic positions were relaxed to minimize the total energy of the molecule and the interatomic forces were partially corrected for van der Waals interactions applying semiempirical dispersion terms.[67,68]

Acknowledgements

The research leading to these results has received funding from the European Research Council under the European Union's Seventh Framework Programme (FP7/2007-2013)/ERC (grant number 259297). The authors thank the CNRS, the Université Paris Sud 11 and the CEA for financial support. The research described here has been also supported by Triangle de la Physique project "SpinMol" (22001100-003344T), the ANR project MolNanoSpin (08-NANO-P110-48), the ANR project Nanocrisnet (ANR-11-BS10-018) and the Cnano Région Ile de France. This work is also supported by a public grant overseen by the French National Research Agency (ANR) as part of the "Investissements d'Avenir" program "Labex NanoSaclay" (reference: ANR-10-LABX-0035).

Keywords: dipolar interaction · salen · scanning tunneling microscopy · self-assembly · synthesis

[1] K. Seufert, M.-L. Bocquet, W. Auwärter, A. Weber-Bargioni, J. Reichert, N. Lorente, J. V. Barth, *Nat. Chem.* **2011**, *3*, 114–119.
[2] T. Komeda, H. Isshiki, J. Liu, K. Katoh, M. Shirakata, B. K. Breedlove, M. Yamashita, *ACS Nano* **2013**, *7*, 1092–1099.
[3] F. Sedona, M. Di Marino, D. Forrer, A. Vittadini, M. Casarin, A. Cossaro, L. Floreano, A. Verdini, M. Sambi, *Nat. Mater.* **2012**, *11*, 970–977.
[4] C. Krull, R. Robles, A. Mugarza, P. Gambardella, *Nat. Mater.* **2013**, *12*, 337–343.
[5] T. Miyamachi, M. Gruber, V. Davesne, M. Bowen, S. Boukari, L. Joly, F. Scheurer, G. Rogez, T. K. Yamada, P. Ohresser, E. Beaurepaire, W. Wulfhekel, *Nat. Commun.* **2012**, *3*, 938.
[6] J. Schwöbel, Y. S. Fu, J. Brede, A. Dilullo, G. Hoffmann, S. Klyatskaya, M. Ruben, R. Wiesendanger, *Nat. Commun.* **2012**, *3*, 953.
[7] K. J. Franke, G. Schulze, J. I. Pascual, *Science* **2011**, *332*, 940–944.
[8] V. A. Dediu, L. E. Hueso, I. Bergenti, C. Taliani, *Nat. Mater.* **2009**, *8*, 707–716.
[9] L. Bogani, W. Wernsdorfer, *Nat. Mater.* **2008**, *7*, 179–186.

© 2014 Wiley-VCH Verlag GmbH & Co. KGaA, Weinheim

[10] X. Chen, Y. S. Fu, S. H. Ji, T. Zhang, P. Cheng, X. C. Ma, X. L. Zou, W. H. Duan, J. F. Jia, Q. K. Xue, *Phys. Rev. Lett.* **2008**, *101*, 197208.
[11] F. Rosei, M. Schunack, Y. Naitoh, P. Jiang, A. Gourdon, E. Laegsgaard, I. Stensgaard, C. Joachim, F. Besenbacher, *Prog. Surf. Sci.* **2003**, *71*, 95 – 146.
[12] J. V. Barth, *Annu. Rev. Phys. Chem.* **2007**, *58*, 375 – 407.
[13] J. Hieulle, F. Silly, *J. Mater. Chem. C* **2013**, *1*, 4536 – 4539.
[14] R. Azumi, G. Götz, T. Debaerdemaeker, P. Bäuerle, *Chem. Eur. J.* **2000**, *6*, 735 – 744.
[15] P. Zell, F. Mögele, U. Ziener, B. Rieger, *Chem. Eur. J.* **2006**, *12*, 3847 – 3857.
[16] S. Vijayaraghavan, D. Ecija, W. Auwärter, S. Joshi, K. Seufert, M. Drach, D. Nieckarz, P. Szabelski, C. Aurisicchio, D. Bonifazi, J. V. Barth, *Chem. Eur. J.* **2013**, *19*, 14143 – 14150.
[17] D. Jewell, S. J. Kyran, D. Rabinovich, E. C. H. Sykes, *Chem. Eur. J.* **2012**, *18*, 7169 – 7178.
[18] L. Zöphel, K. S. Mali, P. S. Reddy, M. Wagner, S. De Feyter, W. Pisula, K. Müllen, *Chem. Eur. J.* **2012**, *18*, 3264 – 3276.
[19] D. Bonifazi, S. Mohnani, A. Llanes-Pallas, *Chem. Eur. J.* **2009**, *15*, 7004 – 7025.
[20] K. S. Mali, K. Lava, K. Binnemans, S. De Feyter, *Chem. Eur. J.* **2010**, *16*, 14447 – 14458.
[21] P. Donovan, A. Robin, M. S. Dyer, M. Persson, R. Raval, *Chem. Eur. J.* **2010**, *16*, 11641 – 11652.
[22] M. Matena, M. Stöhr, T. Riehm, J. Björk, S. Martens, M. S. Dyer, M. Persson, J. Lobo-Checa, K. Müller, M. Enache, H. Wadepohl, J. Zegenhagen, T. A. Jung, L. H. Gade, *Chem. Eur. J.* **2010**, *16*, 2079 – 2091.
[23] C. Lu, E. K. Zhu, Y. D. Liu, Z. Y. Liu, Y. F. Lu, J. L. He, D. L. Yu, Y. J. Tian, B. Xu, *J. Phys. Chem. C* **2010**, *114*, 3416 – 3421.
[24] M. Mura, X. Sun, F. Silly, H. T. Jonkman, G. A. D. Briggs, M. R. Castell, L. N. Kantorovich, *Phys. Rev. B* **2010**, *81*, 195412.
[25] Q. H. Wang, M. C. Hersam, *Nat. Chem.* **2009**, *1*, 206 – 211.
[26] D. Écija, K. Seufert, D. Heim, W. Auwärter, C. Aurisicchio, C. Fabbro, D. Bonifazi, J. V. Barth, *ACS Nano* **2010**, *4*, 4936 – 4942.
[27] S. Uemura, M. Aono, T. Komatsu, M. Kunitake, *Langmuir* **2011**, *27*, 1336 – 1340.
[28] M. Mura, F. Silly, G. A. D. Briggs, M. R. Castell, L. N. Kantorovich, *J. Phys. Chem. C* **2009**, *113*, 21840 – 21848.
[29] J. Otsuki, *Coord. Chem. Rev.* **2010**, *254*, 2311 – 2341.
[30] G. Salassa, M. J. J. Coenen, S. J. Wezenberg, B. L. M. Hendriksen, S. Speller, J. A. A. W. Elemans, A. W. Kleij, *J. Am. Chem. Soc.* **2012**, *134*, 7186 – 7192.
[31] J. Elemans, S. J. Wezenberg, M. J. J. Coenen, E. C. Escudero-Adan, J. Benet-Buchholz, D. den Boer, S. Speller, A. W. Kleij, S. De Feyter, *Chem. Commun.* **2010**, *46*, 2548 – 2550.
[32] S. Kuck, S. H. Chang, J. P. Klockner, M. H. Prosenc, G. Hoffmann, R. Wiesendanger, *ChemPhysChem* **2009**, *10*, 2008 – 2011.
[33] M. T. Räisänen, F. Mogele, S. Feodorow, B. Rieger, U. Ziener, M. Leskela, T. Repo, *Eur. J. Inorg. Chem.* **2007**, 4028 – 4034.
[34] C. Hirel, K. E. Vostrikova, J. Pécaut, V. I. Ovcharenko, P. Rey, *Chem. Eur. J.* **2001**, *7*, 2007 – 2014.
[35] C. J. Whiteoak, G. Salassa, A. W. Kleij, *Chem. Soc. Rev.* **2012**, *41*, 622 – 631.
[36] L. Canali, D. C. Sherrington, *Chem. Soc. Rev.* **1999**, *28*, 85 – 93.
[37] P. G. Cozzi, *Chem. Soc. Rev.* **2004**, *33*, 410 – 421.
[38] S.-C. Xiang, Z. Zhang, C.-G. Zhao, K. Hong, X. Zhao, D.-R. Ding, M.-H. Xie, C.-D. Wu, M. C. Das, R. Gill, *Nat. Commun.* **2011**, *2*, 204.
[39] A. Chellamani, N. Ismail Alhaji, S. Rajagopal, R. Sevvel, C. Srinivasan, *Tetrahedron* **1995**, *51*, 12677 – 12698.
[40] E. Baciocchi, O. Lanzalunga, B. Pirozzi, *Tetrahedron* **1997**, *53*, 12287 – 12298.
[41] V. K. Sivasubramanian, M. Ganesan, S. Rajagopal, R. Ramaraj, *J. Org. Chem.* **2002**, *67*, 1506 – 1514.
[42] R. Sevvel, S. Rajagopal, C. Srinivasan, N. I. Alhaji, A. Chellamani, *J. Org. Chem.* **2000**, *65*, 3334 – 3340.
[43] N. S. Venkataramanan, S. Premsingh, S. Rajagopal, *J. Org. Chem.* **2003**, *68*, 7460 – 7470.
[44] B. Saito, T. Katsuki, *Tetrahedron Lett.* **2001**, *42*, 8333 – 8336.
[45] N. S. Venkataramanan, G. Kuppuraj, S. Rajagopal, *Coord. Chem. Rev.* **2005**, *249*, 1249 – 1268.
[46] A. DiLullo, S.-H. Chang, N. Baadji, K. Clark, J-P Klöckner, M.-H. Prosenc, S. Sanvito, R. Wiesendanger, G. Hoffmann, S.-W. Hla, *Nano Lett.* **2012**, *12*, 3174 – 3179.
[47] M. Viciano-Chumillas, J. Hieulle, T. Mallah, F. Silly, *J. Phys. Chem. C* **2012**, *116*, 23404 – 23407.
[48] J. N. Hohman, P. Zhang, E. I. Morin, P. Han, M. Kim, A. R. Kurland, P. D. McClanahan, V. P. Balema, P. S. Weiss, *ACS Nano* **2009**, *3*, 527 – 536.
[49] L. Xu, X. Miao, X. Ying, W. Deng, *J. Phys. Chem. C* **2012**, *116*, 1061 – 1069.
[50] W. Tong, Y. Wei, K. W. Armbrust, M. B. Zimmt, *Langmuir* **2009**, *25*, 2913 – 2923.
[51] Y. Wei, W. Tong, M. B. Zimmt, *J. Am. Chem. Soc.* **2008**, *130*, 3399 – 3405.
[52] J. B. Patterson, D. G. Lonergan, US Patent Application Publication 2008/154484-A1, **2008**.
[53] F. Silly, *J. Microsc.* **2009**, *236*, 211 – 218.
[54] J. P. Lewis, K. R. Glaesemann, G. A. Voth, J. Fritsch, A. A. Demkov, J. Ortega, O. F. Sankey, *Phys. Rev. B* **2001**, *64*, 195103.
[55] P. Jelínek, H. Wang, J. P. Lewis, O. F. Sankey, J. Ortega, *Phys. Rev. B* **2005**, *71*, 235101.
[56] O. F. Sankey, D. J. Niklewski, *Phys. Rev. B* **1989**, *40*, 3979 – 3995.
[57] J. P. Lewis, P. Jelínek, J. Ortega, A. A. Demkov, D. G. Trabada, B. Haycock, H. Wang, G. Adams, J. K. Tomfohr, E. Abad, et al., *Phys. Status Solidi B* **2011**, *248*, 1989 – 2007.
[58] J. Harris, *Phys. Rev. B* **1985**, *31*, 1770 – 1779.
[59] W. M. C. Foulkes, R. Haydock, *Phys. Rev. B* **1989**, *39*, 12520 – 12536.
[60] M. Basanta, Y. Dappe, P. Jelinek, J. Ortega, *Comput. Mater. Sci.* **2007**, *39*, 759 – 766.
[61] A. A. Demkov, J. Ortega, O. F. Sankey, M. P. Grumbach, *Phys. Rev. B* **1995**, *52*, 1618 – 1630.
[62] Y. J. Dappe, M. A. Basanta, F. Flores, J. Ortega, *Phys. Rev. B* **2006**, *74*, 205434.
[63] Y. J. Dappe, J. Ortega, F. Flores, *Phys. Rev. B* **2009**, *79*, 165409.
[64] P. Giannozzi, S. Baroni, N. Bonini, N. M. Calandra, R. Car, C. Cavazzoni, D. Ceresoli, G. L. Chiarotti, M. Cococcioni, I. Dabo, A. Dal Corso, S. Fabris, G. Fratesi, S. de Gironcoli, R. Gebauer, U. Gerstmann, C. Gougoussis, A. Kokalj, M. Lazzeri, L. Martin-Samos, N. Marzari, F. Mauri, R. Mazzarello, S. Paolini, A. Pasquarello, L. Paulatto, C. Sbraccia, S. Scandolo, G. Sclauzero, A. P. Seitsonen, A. Smogunov, P. Umari, R. M. Wentzcovitch, *J. Phys. Condens. Matter* **2009**, *21*, 395502.
[65] J. P. Perdew, K. Burke, M. Ernzerhof, *Phys. Rev. Lett.* **1996**, *77*, 3865 – 3868.
[66] D. Vanderbilt, *Phys. Rev. B* **1990**, *41*, 7892 – 7895.
[67] S. Grimme, *J. Comput. Chem.* **2006**, *27*, 1787 – 1799.
[68] V. Barone, M. Casarin, D. Forrer, M. Pavone, M. Sambi, A. Vittadini, *J. Comp. Chem.* **2009**, *30*, 934 – 939.

Received: April 19, 2014
Revised: June 16, 2014
Published online on September 15, 2014

© 2014 Wiley-VCH Verlag GmbH & Co. KGaA, Weinheim